Results in Chemistry 4 (2022) 100421

Contents lists available at ScienceDirect

Results in Chemistry

journal homepage: www.sciencedirect.com/journal/results-in-chemistry

Protonation induced self-complementarity of rod-like Cu(NTA)(bpeH) units and their layered supramolecular self-assembly entrapping heptamer like water clusters

Debabrata Singha [a], Sirajuddin Sarkar [b], Nilasish Pal [c,*], Atish Dipankar Jana [b,*]

[a] Department of Chemistry, Physical Chemistry Section, Visva-Bharati University, Santiniketan, Birbhum 731235, West Bengal, India
[b] Department of Physics, Behala College, Parnashree, Kolkata 700060, West Bengal, India
[c] Department of Chemistry, Seth Anandram Jaipuria College, 10, Raja Nabakrishna Street, Kolkata 700005, West Bengal, India

ARTICLE INFO

Keywords:
Water heptamer cluster
Heptamer mimic
NTA
Bpe
Hydrogen bonding interaction
Hydrophobic cavity

ABSTRACT

Molecular self-assembly is the most important methodology for synthesizing novel materials including nano-materials. The ultimate challenge for scientists is to predict the self-assembled pattern of a set of molecular components. The labile nature of self-assembly arises from weak intermolecular forces which makes the outcome diverse, as small changes in physicochemical condition changes the course of self-assembly strongly. A one-pot reaction of 1,2-bis(4-pyridyl)ethylene (bpe), potassium salt of nitrilo-tri-acetic acid (K_3NTA) and basic $CuCO_3$ in an acidic medium (around *p*H = 4) give rise to a metal–organic complex with molecular formula $C_{18}H_{17}CuN_3O_6.6(H_2O)$ (henceforth it will be referred to as Cu-NTA-bpeH, where bpeH is singly protonated 1,2-bis(4-pyridyl)ethylene) whose self-assembly in the solid state shows that even a simple protonation event can drastically influence the course of the self-assembly. Further complication may arise from the participation of solvent water molecules in an unpredictable manner like the appearance of a new water-carboxylate heptamer cluster in the present crystal structure. The study of this simple system shows that *p*H-controlled protonation can lead to self-complementary metal organic units with interesting supramolecular architecture. The self-assembled system has been characterized by X-ray structural studies, Hirshfeld fingerprint and surface analysis, DFT computational studies as well as TG-DTA studies. The present crystal, which is analogous to clathrate hydrate, can possibly act as gas absorption and storage medium for future use.

Introduction:

During current times molecular self-assembly has become a prominent methodology in materials science towards realization of advanced materials [1,2]. Materials scientists are trying to adopt this ubiquitous spontaneous process prevalent in the biological world [3,4] with an aim to replicate the sophistication and complexity of biomaterials in artificially synthesized systems. The bottom-up assembly of nano-materials and nano-scale functional devices have mainly relied on the self-assembly process [5,6] which can be directed to achieve a desired pattern. Self-assembly is also inherent to the process of growth of crystalline solids which according to Dunitz, is "supermolecules per excellence" [7]. In the area of "crystal engineering" [8–10], the professed goal is the synthesis of designed crystalline solids with intended functional properties. The targeted achievement of the desired self-assembled pattern is beset with tremendous challenges due the labile nature of the self-assembly process which are mainly governed by the weak inter molecular forces [11] like hydrogen bonding [12], π-stacking interaction [13–15], *van der* Waals interaction [16] etc. Though the challenge is great due to weak nature of the forces involved, it is simultaneously a blessing of kind as the weak nature of interaction forces allows easier assembly and deassembly of components. This is a prerequisite for many dynamic self-assembled systems like sensors and devices which rely on multi step processes mimicking biochemical processes [17,18]. Molecular recognition between complementary units is fundamental to self-assembly process [19,20]. Identification of robust self-assembling motifs and understanding the stability of such motifs by estimating their binding energies has become quite useful in the pursuit of designing self-assembled systems. In this regard exploration and identification of the recurring self-assembling motifs which are

* Corresponding authors.
E-mail addresses: np.chemistry@sajaipuriacollege.ac.in (N. Pal), atish-dipankar@behalacollege.in (A.D. Jana).

https://doi.org/10.1016/j.rechem.2022.100421
Received 31 March 2022; Accepted 27 June 2022
Available online 30 June 2022
2211-7156/© 2022 The Author(s). Published by Elsevier B.V. This is an open access article under the CC BY-NC-ND license (http://creativecommons.org/licenses/by-nc-nd/4.0/).

inherently stable has become an active subfield in this area. Various physico-chemical parameters like pressure [21], temperature [22], *p*H of the solution [23], molar ratios of reactants [24] as well as different solvents [25] used for carrying out the reaction influence the diverse outcome of the self-assembled systems. The *p*H of reaction medium is often easy to control and *p*H dependent diversity in the self-assembly is exemplified by different polymorphs observed in many crystalline systems [26]. Another hurdle in the way of predicting crystal structure is the insufficient knowledge regarding water of crystallization. Influence of water molecules in molecular self-assembly is becoming crucial [27,28] in the present era of nano-science and technology as nanometric precession is very much important. Insights regarding the behaviour of water in nano-confinement can be obtained through the study of small water clusters trapped in crystalline materials are during crystallization [29,30]. Often water clusters with new and unforeseen topology are discovered during X-ray structure determination. In the present paper we report a new molecular complex whose self-assembly is enforced by the *p*H controlled protonation of the bis-pyridyl ethylene (bpe) ligand used to design the Cu(II) based molecular complex which renders self-complementarity of the molecular unit. We also report a new heptamer water-carboxylate cluster [Scheme 1] which acts as three dimensional supramolecular pillars for the self-assembled 2D layers of the Cu-NTA-bepH units. Besides the Hirshfeld surface analysis and TG-DTA study, electronic structural analysis of the Cu-NTA-bpeH complex has been explored through DFT methodology.

Experimental

Material and methods

All solvents and reagents were obtained commercially and used without further purification. Infrared (IR) spectroscopic studies have been carried out with Perkin-Elmer Spectrum one using KBr pellet. The thermal study has been carried out with Perkin Elmer STA 6000 Simultaneous Thermal Analyzer.

Synthesis

5 ml aqueous solution of K_3NTA (305 mg, 1 mmol) was added drop wise to an ethanolic solution (5 ml) of 1,2-bis(4-pyridyl)ethylene (182 mg, 1 mmol) while stirring. 5 ml aqueous solution of basic $CuCO_3$ (110 mg, 0.5 mmol) was added drop wise to the reaction mixture which became blue after addition of dilute HCl (*p*H ~ 4.0). This mixture was then stirred for 3 h after which it was filtered. The filtrate was left for slow evaporation and after a few days, blue coloured block-shaped crystals appeared with 70% yield. Obtained crystals are unstable at room temperature when these are taken out of the mother solution. The crystals become opaque and colourless within approximately thirty minutes of exposure to air [Fig. S2, Fig. S3]. **Yield:** 70%, **IR (KBr):** 3446, 2928, 1613, 1390, 912, 827 cm^{-1}, **UV (H_2O):** λ_{max}: 222, 299 nm (Fig. S1).

X-ray crystallography

Diffraction intensities for the complex **1** were collected at 293(2)K on a Bruker Kappa Apex-II CCD area-detector diffractometer (MoK$_\alpha$, λ = 0.71073 Å). The structure was solved by the direct method and refined with a full-matrix least-squares technique using the SHELXL-2021.3 program package [31]. Empirical absorption correction was applied. Anisotropic thermal parameters were used for all the non-hydrogen atoms. The hydrogen atoms were generated from riding atom model. Crystal data, details of data collection and refinement for the complex **1** has been summarized in Table 1. Selected bond distances and bond angles are listed in Table 2, hydrogen bonding interaction data in Table 3.

Table 1
Crystal data and Refinement parameters.

Crystal Data	
CCDC NO.	1947087
Formula	$C_{18}H_{17}CuN_3O_6.6(H_2O)$
Formula Weight	542.99
Crystal System	Triclinic
Space group	$P\bar{1}$ (No. 2)
a, b, c [Å]	7.7458(9) 11.9205(12) 13.6155(12)
α, β, γ [°]	66.512(9) 82.704(8) 79.935(9)
V [Å^3]	1133.0(2)
Z	2
D(calc) [g/cm^3]	1.592
μ(MoK$_\alpha$) [/mm]	1.033
F(000)	566
Crystal Size [mm]	0.20 × 0.18 × 0.11
Data Collection	
Temperature (K)	293
Radiation [Å]	MoK$_\alpha$ 0.71073
Theta Min-Max [°]	1.6, 25.0
Dataset	−9: 9; −14: 14; −16: 16
Tot., Uniq. Data, R(int)	19,885, 4001, 0.034
Observed data [I > 2.0 σ(I)]	3834
Refinement	
N_{ref}, N_{par}	4001, 359
R, wR_2, S	0.0249, 0.0654, 1.12
Max. and Av. Shift/Error	0.00, 0.00
Min. and Max. Resd. Dens. [e/Å^3]	−0.28, 0.37

$w = 1/[\sigma(F_o^2)+(0.0198P)^2 + 1.2286P]$ where $P = (F_o^2 + 2F_c^2)/3$.

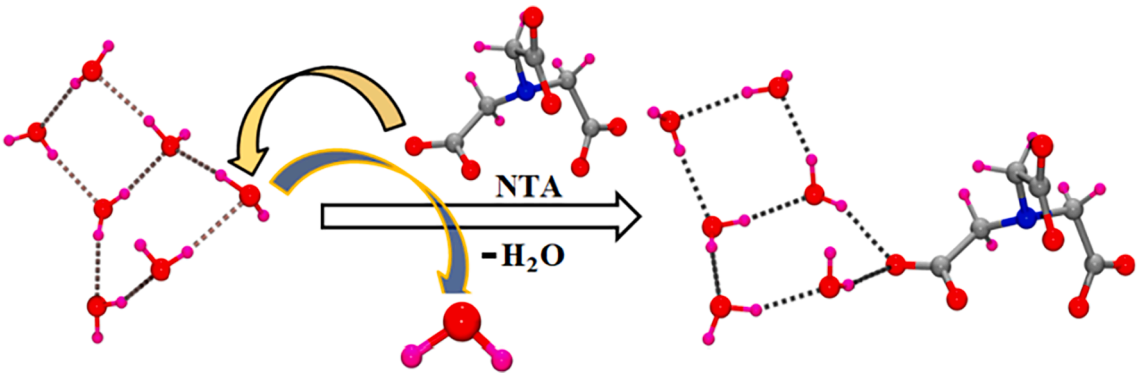

Scheme 1. Carboxylate O atom of nitrilo-tri-acetate (NTA) replacing a water molecule in the heptamer water cluster.

Table 2
Selected bond distance and bond angle (Å, °).

Bond Distances			
Cu1-O1	1.9873(14)	N1-C4	1.4880(2)
Cu1-O4	2.0067(15)	N1-C6	1.4800(3)
Cu1-O6	2.1417(15)	N2-C7	1.3450(3)
Cu1-N1	1.9985(16)	N2-C11	1.3450(3)
Cu1-N2	1.9634(17)	N3-C16	1.3340(3)
N1-C2	1.4850(2)	N3-C17	1.3420(3)
Bond Angles			
O1-Cu1-O4	137.70(6)	Cu1-N1-C4	105.20(12)
O1-Cu1-O6	107.34(6)	Cu1-N1-C6	106.92(11)
O4-Cu1-O6	110.80(6)	Cu1-N2-C7	123.50(13)
O1-Cu1-N1	85.74(6)	Cu1-N2-C11	117.35(15)
O1-Cu1-N2	99.21(7)	N1-Cu1-N2	174.75(7)
O4-Cu1-N1	82.31(6)	Cu1-O1-C1	113.77(13)
O4-Cu1-N2	92.80(6)	Cu1-O4-C3	112.24(11)
O6-Cu1-N1	81.74(6)	Cu1-O6-C5	111.20(12)
O6-Cu1-N2	98.33(6)	Cu1-N1-C2	106.93(12)

Table 3
Hydrogen bond table (Å, °).

D-H···A	D-H (Å)	H···A (Å)	D···A (Å)	<D-H···A (°)	symmetry
O1W-H1W1···O4	0.85 (4)	1.96(4)	2.806 (2)	170(4)	
O1W-H2W1···O5	0.81 (3)	2.06(3)	2.861 (2)	168(3)	1 + x,y,z
O2W-H1W2···O1W	0.88 (3)	1.90(3)	2.730 (2)	158(3)	
O2W-H2W2···O6	0.82 (4)	2.06(4)	2.867 (2)	169(4)	1-x,1-y,1-z
O3W-H1W3···O2W	0.77 (3)	2.01(3)	2.777 (3)	171(3)	
O3W-H2W3···O6W	0.85 (4)	1.97(4)	2.819 (3)	171(4)	2-x,1-y,-z
O4W-H1W4···O3W	0.75 (4)	2.03(3)	2.771 (3)	172(4)	
O4W-H2W4···O5	0.84 (4)	2.34(4)	3.067 (3)	146(3)	
O5W-H1W5···O3	0.86 (3)	1.90(3)	2.753 (2)	175(3)	
O5W-H2W5···O4W	0.82 (3)	2.11(3)	2.904 (3)	164(3)	2-x, 1-y,-z
O6W-H1W6···O5W	0.89 (4)	1.96(3)	2.794 (2)	156(3)	
O6W-H2W6···O5	0.79 (3)	2.06(3)	2.798 (2)	155(3)	1-x,1-y,-z
N3-H3N···O2	0.83 (3)	1.89(2)	2.688 (2)	164(2)	1 + x,y,1 + z
C4-H4A···O1	0.97	2.58	3.490 (3)	156	1-x, 2-y,-z
C4-H4A···O2	0.97	2.60	3.151 (3)	117	1-x, 2-y,-z
C6-H6A···O5W	0.97	2.50	3.267 (3)	136	2-x, 1-y,-z
C10-H10···O5	0.93	2.42	3.339 (3)	169	1-x,1-y,1-z
C13-H13···O3W	0.93	2.57	3.472 (3)	164	X,1 + y,z
C15-H15···O2W	0.93	2.56	3.412 (3)	153	X,1 + y,z
C16-H16···O1W	0.93	2.52	3.399 (3)	158	2-x,2-y, 1-z
C17-H17···O3	0.93	2.49	3.356 (3)	156	x,y,1 + z
C18-H18···O6W	0.93	2.31	3.215 (3)	165	x,y,1 + z
C2-H2A···O3	0.97	2.38	3.338 (2)	170	−1 + x,y,z

Hirshfeld surface analysis

Hirshfeld surface analysis [14,15,32–37] is a useful technique that helps in quantifying and visualizing intermolecular interactions. This analysis is based on electron density distribution in which atoms are assumed as spherical entities [38]. For a given crystal structure the Hirshfeld surface is a unique one. The computation of Hirshfeld surface is based on the normalized contact distance d_{norm} which in turn is dependent on d_i, d_e and *van der* Waals (*vd*W) radii of the atom. Here, d_i is the distance to the nearest nucleus internal to the surface and d_e is the distance from the point to the nearest nucleus external to the surface. d_i, d_e and *van der* Waals (*vd*W) radii are related with each other according to equation (1). On the d_{norm} surface, red spots indicate strong intermolecular interaction region though C-H···O interactions which have higher contact distances have corresponding smaller area on the surface. On the other hand, blue spots indicate regions with contact distances longer than vdW separation corresponding [39,40]. Two-dimensional (2D) fingerprint plot is complementary to Hirshfeld surface in which various possible d_e values for a given Hirshfeld surface is plotted against d_i values [32,34,41]. This plot uniquely identifies different intermolecular interactions which appear as spikes in this plot. The Hirshfeld surfaces are mapped using d_{norm}. The Hirshfeld surfaces and 2D fingerprint plots presented in this paper have been generated using Crystal-Explorer 2.1 [42].

$$d_{norm} = \frac{d_i - r_i^{vdw}}{r_i^{vdw}} + \frac{d_e - r_e^{vdw}}{r_e^{vdw}} \quad (1)$$

Methodology of theoretical study:

DFT computational studies [43–47] have been performed using the GAUSSIAN-03 package [48]. Initial geometries of the Cu-NTA-bpeH complex and the heptamer water cluster were adopted from the crystal structure which were utilized as the starting configuration in the search of optimized geometry. Calculations have been performed at the DFT/6-311G level of theory using B3LYP hybrid density functional. The binding energy for the heptamer ($B.E._{heptamer}$) water cluster has been estimated as $B.E._{heptamer} = E_{heptamer} - 7{*}E_{H2O}$. Basis set superposition error has been estimated using Counterpoise method.

Result and discussion

Structural description

A possible reaction towards the formation of the title complex has been shown in Scheme 2. Cu(II) ion, potassium salt of nitrilo triacetic acid and bpe form the title complex in a acidic medium. Single-crystal X-ray structural analysis reveals a mononuclear coordination complex of Cu(II), nitrilotriacetate and protonated bis-pyridyl ethylene and six lattice water molecules (Fig. 1a). These units crystallize in triclinic $P\bar{1}$ (No. 2) space group. The molecular formula of the crystalline complex is [Cu(II)(bpeH)(NTA)].6H_2O. NTA ligand has inherent compatibility for C_3 symmetric metal complexes due to which it is utilized in crystal engineers to induce the trigonal bipyramidal coordination geometry. Though, in many cases NTA binds metal centre utilizing only one or two carboxylate terminals [49,50] instead of all three carboxylate groups besides the central N atom, in the present complex use of NTA has led to a trigonal bipyramidal coordination geometry of Cu(II). Three equatorial coordination sites of Cu(II) have been fulfilled by three carboxylate O atoms (O1, O4, O6) of NTA whereas two axial coordination sites of Cu (II) have been occupied by the central N (N1) atom of NTA and one of the pyridine N atoms (N2) of bpeH. It is interesting to note that the control of the acidity of the reaction medium has led to the protonation of the uncoordinated N atom (N3) of bpe. In the previous instances [51,52] when bpe and NTA were simultaneously utilized to synthesize Cu(II) complexes, dinuclear or trinuclear Cu(II) complexes were

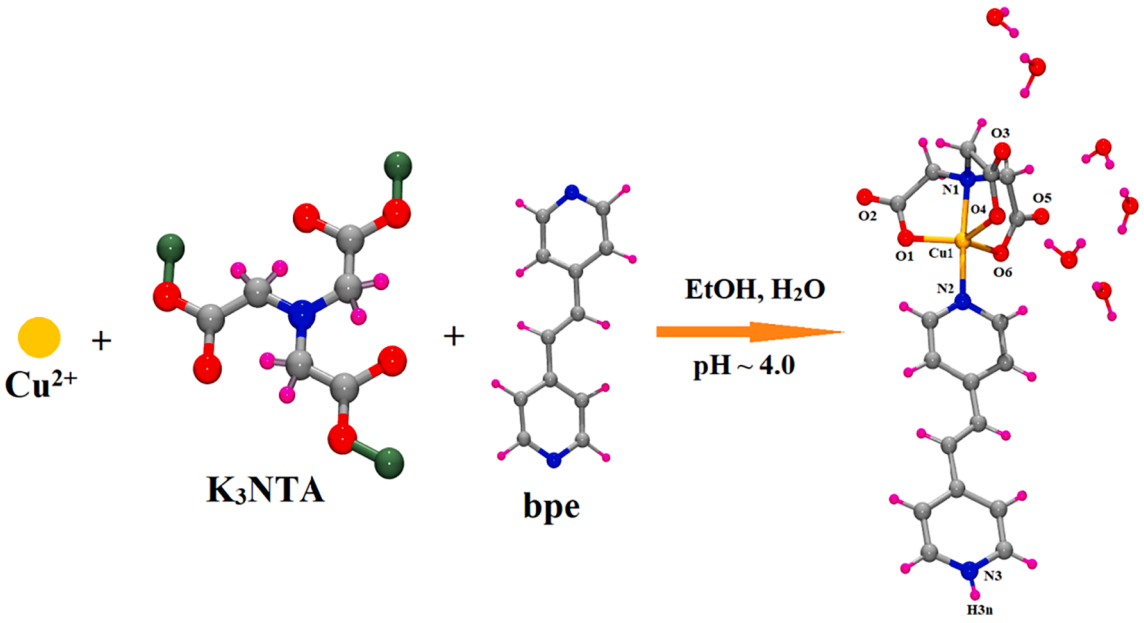

Scheme 2. Reaction between Basic $CuCO_3$, K_3NTA and 1,2-bis(4-pyridyl)ethylene in acidic medium (*p*H ~ 4.0).

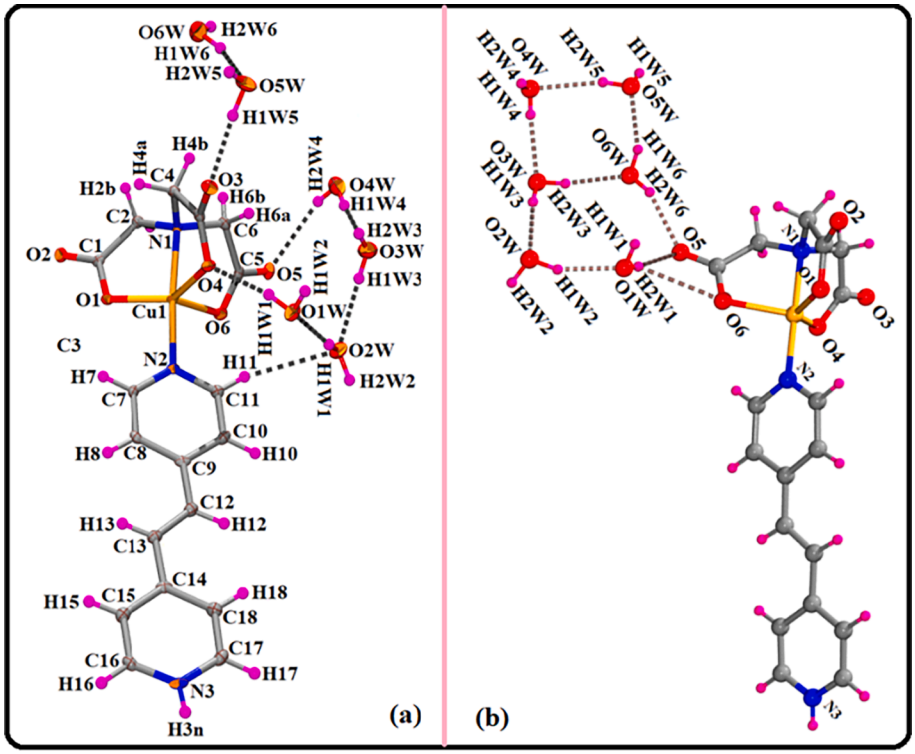

Fig. 1. (a) ORTEP diagram (50% ellipsoidal probability) of the Cu(II) complex with atom numbering scheme (lattice water molecules have been omitted for clarity). (b) Self-association of water molecules in the form of a water heptamer where one of the water molecules has been replaced by carboxylate O (O5) atom.

obtained in all cases. So it can be assumed that controlling *p*H of reaction medium is responsible for mononuclear Cu(II) complex in the present case.

Cu–N and Cu–O coordination bond distances in the present complex are typical of similar Cu(II) complexes reported earlier [51–54]. The Cu1-N1 (NTA) distance is 1.9985(16)Å and Cu1-N2 (bpe) distance is 1.9634(17)Å. On the other hand, Cu1-O1 distance is 1.9873(14)Å, Cu1-O4 distance is 2.0067(15)Å, Cu1-O6 distance is 2.142(15)Å. The angles subtended by the three coordinated oxygen atoms in basal planes are respectively <O1-Cu1-O4 = 137.70°(6); <O1-Cu1-O6 = 107.34°(6) and <O4-Cu1-O6 = 110.80°(6). Other relevant bond lengths and bond angles are given in Table 2. The structural parameter (τ) for the coordination unit of the complex has a value 0.62 which correspond to trigonal bipyramidal coordination geometry.

Bis-pyridyl-ethylene (bpe) coordinates Cu(II) centre in such a way that it makes an angle of 11.43° with the Cu-N2 axis. The optimized geometry of this complex also reveals such an angular disposition with the corresponding angle 12.63°.

Hydrogen bonding and other weak intermolecular forces are responsible for the hierarchical self-assembly of the present complex. Coordination units are organized into 1D ribbon, which are further united via edge-stacking though hydrogen bonding, giving a 2D supramolecular sheets and finally, these sheets are joined by water bridges present in the intervening space. NTA ligands are intrinsically amenable for taking part in hydrogen bonding interaction through the three carboxylate groups. On the other hand, bpe is prone towards stacking interaction (off-set π-stacking in the present crystal) due to the presence of two pyridyl moieties. Thus, NTA and bpe inherently belong to two differing strengths of supramolecular forces, namely, hydrogen bonding and π-stacking. Hydrogen bonding forces are generally stronger than π-stacking forces. This differing strength usually leads to a supramolecular assembly in different directions; stronger force propagates assembly in one particular direction and weaker force in another direction giving rise to anisotropic properties. The water molecules themselves form a cluster and take part in this self-assembly process. Six water molecules self-assemble in the form of a water heptamer (Fig. 1b), where one water molecule is replaced by carboxylate O-atom donated by NTA. In a real sense, the cluster found in the present crystal is a water heptamer mimic, even with the participation of a foreign acceptor atom in the water cluster network, the mimic retains the same topology and nearly the same geometry of the corresponding free water heptamer. These water heptamers act as uniting agent (Fig. 2a) for adjacent supramolecular ladders of coordination units running along the crystallographic *a*-axis (Fig. 2b). The heptamer water cluster consists of two conjoined rings of a water tetramer and a water pentamer mimic. In the pentamer part, one of the water molecules of a pure water pentamer can be assumed as replaced by one of the carboxylate O atom (O5) of NTA (Fig. 2a). The tetramer and the pentamer part share a common edge formed by two water molecules (O3W and O6W). Four water molecules (O3W, O4W, O5W and O6W) form a homodromic h40 planar water tetramer [55,56], where the hydrogen atoms in the hydrogen bonded circuit are aligned successively in the same direction (anticlockwise in Fig. 1b). The h40 tetramer has a distorted rectangular geometry with O4W-O5W distance 2.904(3)Å, O3W-O6W distance 2.819(3)Å, O3W-O4W distance 2.771(3)Å and O5W-O6W distance 2.794(2)Å. The pentamer mimic has geometry very close to that of a pure water cluster pentamer. In a pure water cluster pentamer, four water molecules lie in a single plane and the fifth water molecule is slightly away, up or down of the mean plane passing through the other four water molecules. In the present water pentamer mimic four water molecules O1W, O2W, O3W and O6W lie nearly in the same plane and the oxygen atom O5 is located slightly above this mean plane.

The water clusters actively take part in the supramolecular assembly by bridging diagonally opposite Cu-NTA-bpeH molecular complexes located on two ribbons having a ladder architecture that runs along crystallographic *a*-axis. This has been shown schematically in Fig. 1b. A complementary pair of heptamer mimics hydrogen bond to inversion symmetry related pair of carboxylate terminals (Fig. 2a).

Ligand bpeH molecules have self-assembled among themselves due to hydrogen bonding of the tail of the complex to the head of one such unit in the next ribbon (Fig. 3a). In the ladder assembly whole Cu(NTA)(bpeH) unit behave as a modular unit with a strongly polar head (NTA end containing three carboxylate groups) and a relatively weak polar tail (protonated bpeH molecule) with the central bpe part acing as a hydrophobic region. These units align one by one with head–tail-head–tail alternation and form a supramolecular ladder which extends along the crystallographic *a*-axis. Successive units are glued to each other by weak intermolecular forces, namely, hydrogen bonding (Table 3), lone-pair···π interaction (Fig. 3a). There are four contact points within the oppositely aligned pair of rod-like complexes. Two end contacts are mediated by lone-pair···π interactions between the O atoms contributed by NTA with the protonated pyridyl ring of the bpeH molecule. A tetrad of Cu-NTA-bpeH supramolecular unit is the basic repeating unit of the supramolecular ladder running along the crystallographic *a*-axis (Fig. 3a).

Successive ribbons stack over each other and give rise to a two-dimensional supramolecular sheet of Cu-NTA-bpeH complexes which are the (1 0 1) planes of the crystal. The stacking modes of the ribbon is quite interesting, the trailing edge of one ribbon and the leading edge of the next ribbon are attached to each other through the NTA group mediated hydrogen bonding as well as carbonyl···carbonyl interaction. This gives rise to a step like architecture of the (1 0 1) planes. The details

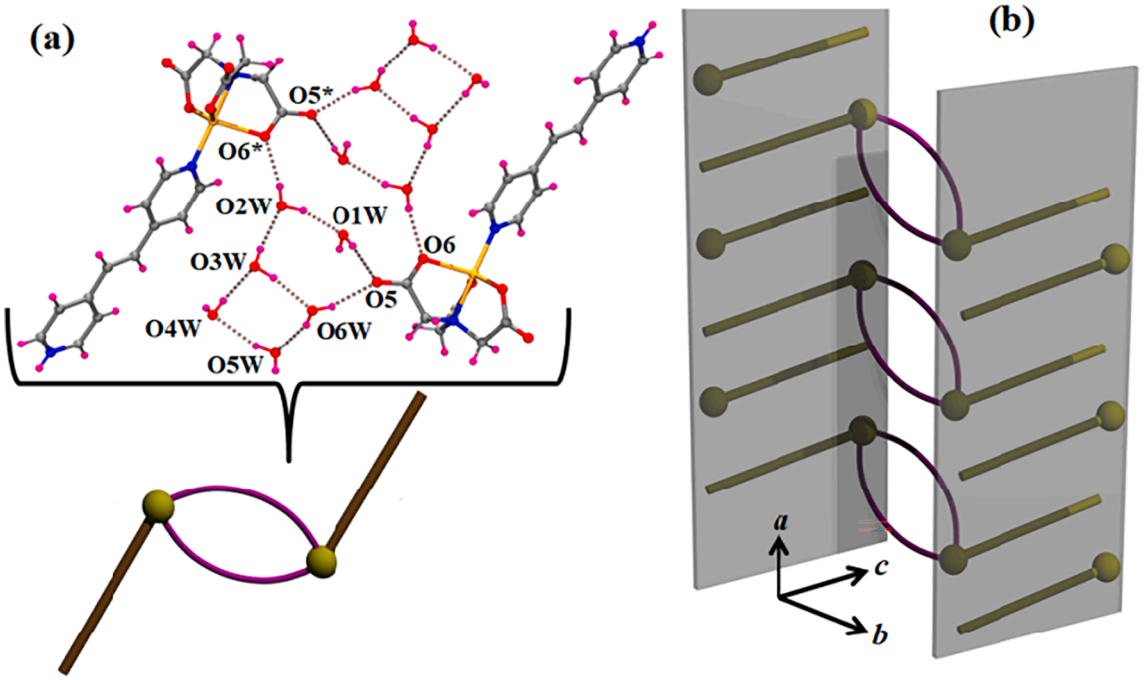

Fig. 2. (a) Water heptamer mimic acting as supramolecular glue in binding two units of CuNTA-bpeH complexes (* = 1-x, 1-y, 1-z) (b) Schematic representation of the corresponding packing of molecular complexes.

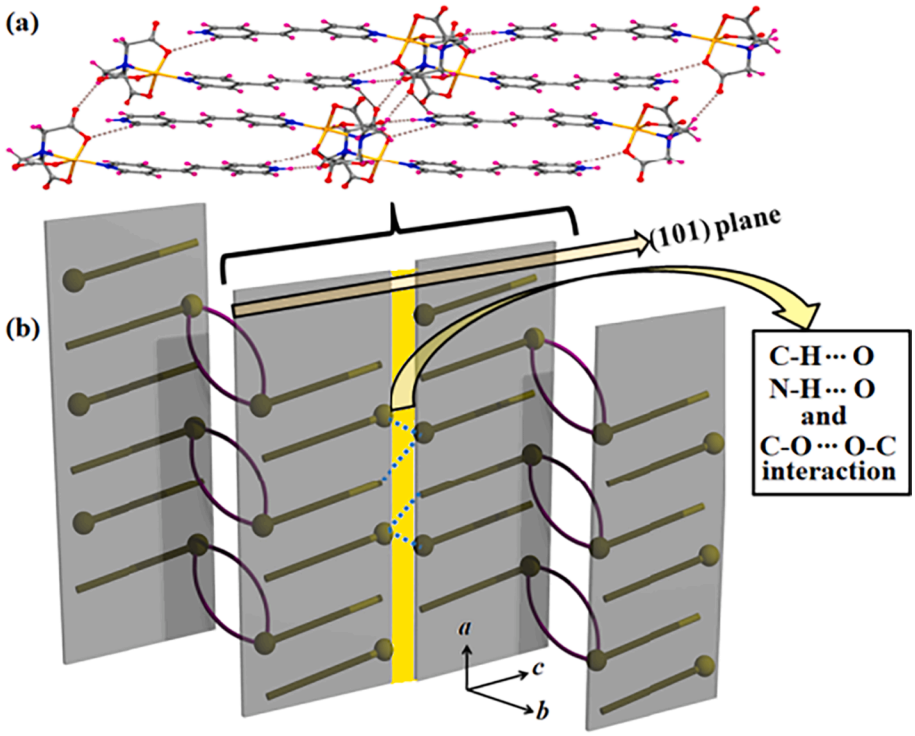

Fig. 3. (a) Supramolecular 2D sheet of NTA units formed through hydrogen bonding interaction. (b) Schematic diagram depicting the packing of layers.

of this NTA-NTA supramolecular interaction have been shown in Fig. 4. There is a synergy of CH···O interaction (Table 3, Table S1) and C-O···O-C interaction. The lone-pair···lone-pair interaction among two carboxylate groups is assisted by CH···O hydrogen bonding interaction (Table 3). This interaction has been corroborated through DFT computation where the optimized geometry of two interacting Cu-NTA-bpeH molecular complexes have been found to be very close to that present in the crystal.

The mutual role of water cluster and the Cu-NTA-bpeH unit in the supramolecular self-assembly is complementary in the present crystal in the sense that for the structural stability of the crystalline state water molecules play a crucial role. We have observed that loss of water molecules from the isolated crystal is spontaneous and this give rise to degradation of crystal quality leading to opaqueness [Fig. S2]. On the other hand, if the crystal is kept immersed within the mother liquor then is quite stable.

To gather a holistic view of the nature of structural and superstructural aspects of CuNTA-bpe complexes we have retrieved similar complexes from the CCDC database (CSD June 2018 release) using ConQuest 1.23. It was surprising that only a handful of Cu-NTA-bpe complexes were reported previously. A review of these complexes reveals that mainly two types of structural varieties are present – either (i) a dinuclear Cu complex or (ii) a trinuclear Cu complex (Scheme SII).

Baolong Li et al. [51] have reported a coordination complex having a molecular formula $[Cu(CH_3COO)(bpe)(H_2O)]_n.n/2[Cu_2(NTA)_2(bpe)].6nH_2O$ where the anionic counter-ions $[Cu_2(NTA)_2(bpe)]^{2-}$ units are dinuclear, in which bpe bridges two Cu(NTA) units rendering it a dumbbell like topology. These two units play a complementary charge balancing role for each other.

Baolong Li et al. [53] reported another system of Cu complexes having formula $[Cu(azpy)(H_2O)_4][Cu_2(NTA)_2(azpy)].6H_2O$. Here, along with NTA, azopyridine was used as a coligand. In this case a cationic coordination polymeric chains of $[Cu(azpy)(H_2O)_4]_n^{n+}$ is supramolecular and anionic $[Cu_2(NTA)_2(azpy)]^{2-}$ dinuclear units act as two distinct entities with complementary charge balancing role for each other. The dinuclear $[Cu_2(NTA)_2(azpy)]^{2-}$ in this complex also has the same dumbbell like topology as that of the $[Cu_2(NTA)_2(bpe)]^{2-}$ units in the $[Cu(CH_3COO)(bpe)(H_2O)]_n.n/2[Cu_2(NTA)_2(bpe)].6nH_2O$ discussed above.

These two systems, exemplify the robust dumbbell topology (Scheme SII) of the $[Cu_2(NTA)_2(L)]^{2-}$ dinuclear units, where L is either bpe or azopyridine. The ligands L here act as bridge between two $Cu(NTA)^{-1}$ units, and it appears that the length of this anionic unit can be tuned by employing other ditopic ligands analogous to bpe or azopyridine.

Baolong Li et al. [54] reported another complex based on Cu, NTA and bpe having a formula $[Cu_3(nta)_2(bpe)_2(H_2O)_4].bpe{\cdot}10H_2O$, where instead of the dinuclear $[Cu(nta)_2(bpe)]^{2-}$, a tri-nuclear neutral $[Cu_3(NTA)_2(bpe)_2(H_2O)_4]$ is present. In this moiety, two units of bpe bridges three Cu centres (Scheme SII) and NTA acts as a capping agent for the two terminal Cu(II) nodes. The middle Cu node is having octahedral coordination geometry with four equatorially coordinated water molecules and *trans* axial sites are coordinated by two bridging bpe units on either side. Two terminal Cu nodes have tbp coordination geometry, whereas the middle Cu node has octahedral coordination geometry. Six units of negative charge of two NTA ligands is balanced by three Cu(II) ions. It appears that the trinuclear topology of the complex, in this case is necessary simply to satisfy the charge neutrality of the whole coordination complex.

In summary, the review of published literature shows that Cu-NTA-bpe system has the propensity to give rise to either a dincular anionic $[Cu_2(NTA)_2(bpe)]^{2-}$ unit, or a trinuclear neutral $[Cu_3(nta)_2(bpe)]$ unit. In contrast, the complex being reported here is a mononuclear Cu complex with formula [Cu(NTA)bpeH], where the protonated bpe along with Cu(II) ion balances the three negative charges of the nta tri-anion. So, the present complex exemplifies a new mode of charge balancing for the Cu-NTA system through ligand protonation which produces the simplest self-contained neutral Cu-NTA-bpeH system. In retrospect, we have looked into the reaction conditions in which the previously reported di or trinuclear Cu-NTA-bpe systems were obtained and the information gathered reveal that for all cases the reactions were carried out in a basic medium (*p*H range 6–11). The reaction we have carried out instead is in an acidic medium (*p*H ~ 4), which can be assumed to be the

causative effect for bpe protonation. So tuning of pH appears to be a key factor for shaping a new topology in Cu-NTA-bpe system.

Protonation of bpe, changed the coordination behaviour of it, instead of a ditopic bridging ligand through coordination to metal nodes, it is now better suited for supramolecular interaction, for hydrogen bonding through the protonated end. This gives rise to the amphiphilic nature of the present metal–organic unit [Cu(NTA)bpeH], rendering it a mesogen like character. NTA end of this mesogen is more polar and acts like the head group of a mesogen, whereas the less polar protonated bpe terminal acts as the tail of the mesogen. This unit is not having the nature of a pure surfactant or a phospholipid molecule with a pure hydrophobic tail and pure head group, instead, both ends are polar with differing amount of polarity and the bpe unit behave as a hydrophobic middle group. Thus, naturally, instead of a cell-wall bilayer assembly or a micellar like spherical assembly we see here more of liquid crystal-like head–tail arrangement giving rise to ribbon- like supramolecular self-assembly of [Cu(NTA)bpeH] metal–organic mesogens. Two edges of this ribbon are strongly polar whereas the middle portion is a line by bpe units, alignment of its edges in a row gives rise to a hydrophobic surface. Edge to edge interaction of successive ribbons give rise to a unique supra-molecular layer in the *ac* plane with alternate polar and non-polar stripes running along *a*-axis. Polar stripes on adjacent layers are doubly bridged by heptamer water clusters whose tetramer units are stabilized in the hydrophobic channels in between adjacent layers.

Theoretical studies

*Optimized geometry of complex **1***

The $[Cu(II)(NTA)]^-$ unit (head part of complex **1**) without bpeH [Fig. S4(a)] as well as the full molecular complex [Cu(II)(NTA)(bpeH)] [Fig. S4(b)] both optimizes and the geometrical parameters of the later nicely matches [Table S2 and S3] with that from the crystal structure. The computed Cu-N_{NTA} distance for this unit agrees very well with that of the crystal structure (Cu-N_{NTA} = 1.9985(16)Å in crystal versus 2.037 Å in computation). The coordination bond strength of the bpeH moiety was estimated as the difference of the energies of the complex 1 and that of the sum of energies of the head part of complex 1 and the bpeH unit. This has come out to be 71.74 kcal/mole [Fig. S5].

Water heptamer mimic and book form water heptamer

The structural stability of the present crystal is strongly dependent on the water molecules. Soon after the crystals are physically taken out of the mother liquor, decomposition of the crystals starts with the appearance of cracks and blue colour of crystals faded out within half an hour. The present heptamer water cluster mimic has an open book like topology resulting from the slightly folded conformation among the pentamer and tetramer cycles in it [Fig. 5a]. It is interesting to note that, the optimized geometry of a pure water only heptamer cluster is really quite close to the geometry of the heptamer mimic present in the crystal structure [Fig. 5]. In this optimized geometry of the water heptamer, the dihedral angle between the mean planes of the pentamer unit and the tetramer unit is 166°. Even with the participation of this O atom the geometry of the heptamer water cluster mimic remains very close to that of the pure heptamer water cluster. The dihedral angle between the pentamer (mimic) plane and the tetramer plane is 157° which is quite close to 166° found computationally for a pure water heptamer. The geometry (O···O distances and O-H···O angles) of the pure heptamer water cluster also do not deviate too much from that of the heptamer mimic (Table S4). We have attempted to estimate the strength of this cooperative interaction among the water molecules of the heptamer water cluster. The basis set superposition error corrected binding energy for the heptamer water cluster has been found to be −54.23 kcal/mole which amounts to −7.75 kcal/mole per water molecule.

Hirshfeld surface analysis

Hirshfeld surface analysis is a useful procedure providing deeper understanding regarding the relative importance of various atom···atom interactions responsible for molecular cohesion within a crystal. The d_{norm} *iso*-surface studded with red spots of varying brightness corresponding to hydrogen bonds between a pair of complementary Cu-NTA-bpeH complexes bridged by heptamer water clusters has been depicted in Fig. 6. Fig. 6(I) shows the Hirshfeld surfaces around Cu-NTA-bpeH units and Fig. 6(II) correspond to the Hirshfeld surface for water cluster bridging these two units. Fig. 6(III) depicts the fingerprint plot corresponding to these interactions. Fig. 6(IV) shows the relative proportion of various weak forces responsible for packing as a pie chart. Details of these interactions have been given as supplementary materials.

TG-DTA study

Thermal decomposition study of the crystalline solid has been depicted in Fig. 7. The thermal study has been carried out in the temperature range 29 °C (room temperature) to 1000 °C. The water of crystallization starts to come out of the solid around 40 °C. Six water molecules are lost in two steps comprising 20% of weight loss. The first step is steeper; containing 10% of weight loss in the temperature range 40–90 °C. In the second step, another 10% of weight loss occurs in the temperature range 90–205 °C due to loss of three remaining water molecules. The water molecules lost in the first step are those water molecules which do not form direct hydrogen bonding contact with any of the carboxylate groups and were responsible for the ordered organization of water molecules in the form of a heptamer. The slow and

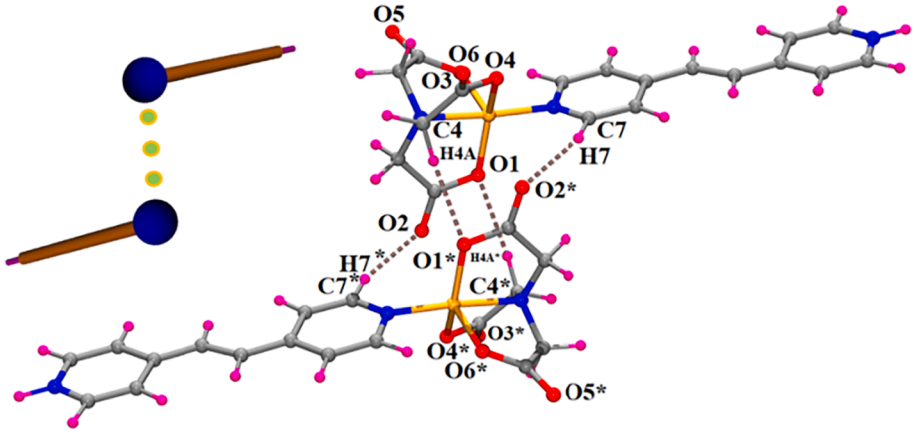

Fig. 4. Hydrogen bonding interaction between two Cu-NTA-bpeH units assembled through CH···O and NTA-NTA interaction at edges (*=1-x, 2-y,-z).

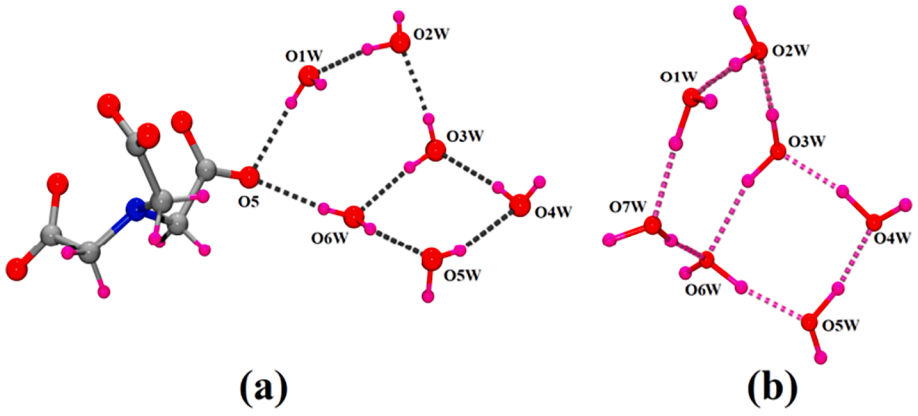

Fig. 5. (a) The water heptamer mimic in comparison to (b) the optimized heptamer water cluster.

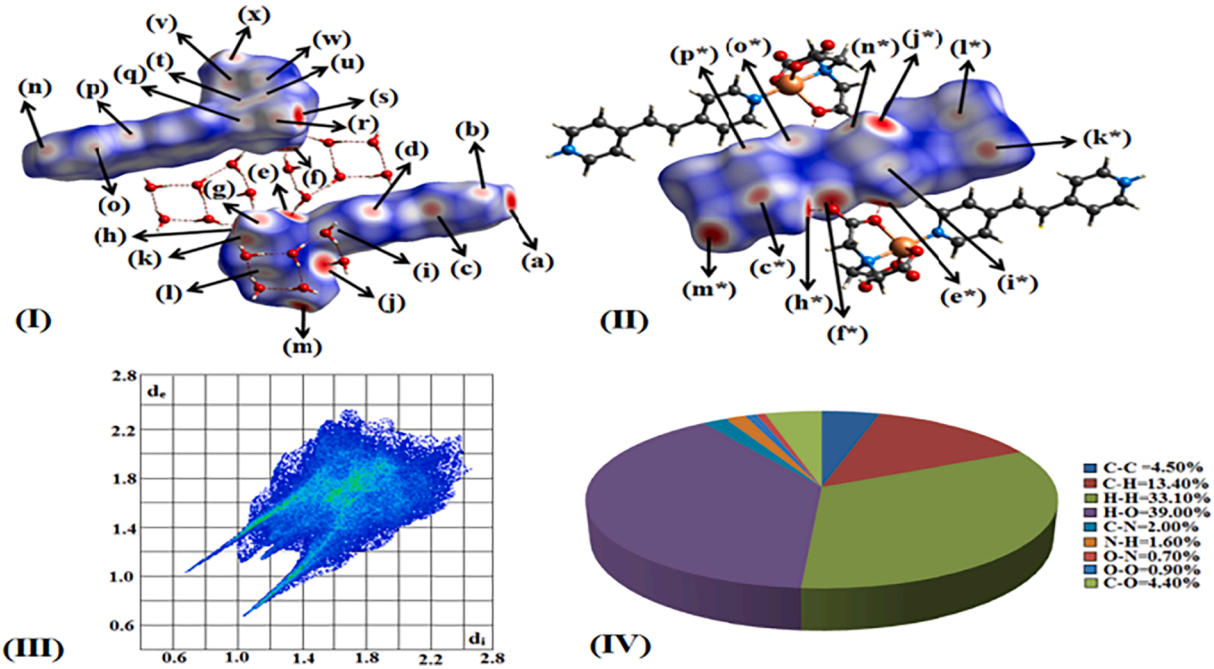

Fig. 6. (I) Hirshfeld surfaces of a pair of molecular complexes with intervening water molecules (II) Hirshfeld surfaces of the intervening water cluster with a pair of molecular complexes (III) fingerprint plot (IV) pie chart depicting relative importance of various weak intermolecular interactions.

sluggish removal of three water molecules in the second step corresponds to those which have direct hydrogen bonding contact with carboxylate groups.

In the third weight loss step bpeH is lost with a weight loss of 33% in a short temperature range from 205–275 °C. In the next step, there is a mass loss of ~17% in the temperature range 275–340 °C. This can be explained by assuming that NTA decomposes through the removal of C, N and hydrogen leaving only oxygen to form Copper-oxide. Copper oxide then slowly loses mass and complete mass loss needs a very high temperature (950 °C). Water loss steps are associated with two distinguishable exotherms corresponding to a reorganization of the crystalline solid (evident in the crystal turning opaque when it is exposed into the open atmosphere). Loss of bpeH, decomposition of NTA and copper-oxide phase transformation all are associated with respective endotherms. Much deeper endotherm corresponding to the decomposition of NTA relative to that of bpeH can possibly be understood from the fact that NTA is a tridentate chelating ligand but bpeH is a monodentate coordinating ligand.

Conclusion

We report here an interesting molecular complex whose self-complementary nature arises from the *p*H induced protonation of the bis-pyridyl ethylene ligand which binds as a monodentate ligand to a Cu (II) centre whose other coordinate sites are satisfied by a tridentate NTA ligand producing a rod like molecular complex. At the lowest level of hierarchy these self-complementary units form a cyclic head to tail supramolecular motif, which repeats periodically giving rise to a 2D supramolecular layer constituted by 1D ladder subunits. Successive supramolecular layers encalthrate water layers in the intervening space which at as bridges joining carboxylate heads of the molecular rod on adjacent layers. Water bridges consists of a unique carboxylate-water hybrid heptamer cluster having open-book topology in which six water molecules and a carboxylate O atom take part. A comparison of DFT computational optimum geometry of the pure water heptamer cluster with that in the crystal structure reveals that even inside the crystal the water-heptamer cluster tends to retain nearly the same geometry as that of a free water heptamer. Water molecules in the present crystal actively take part in the supramolecular assembly by augmenting

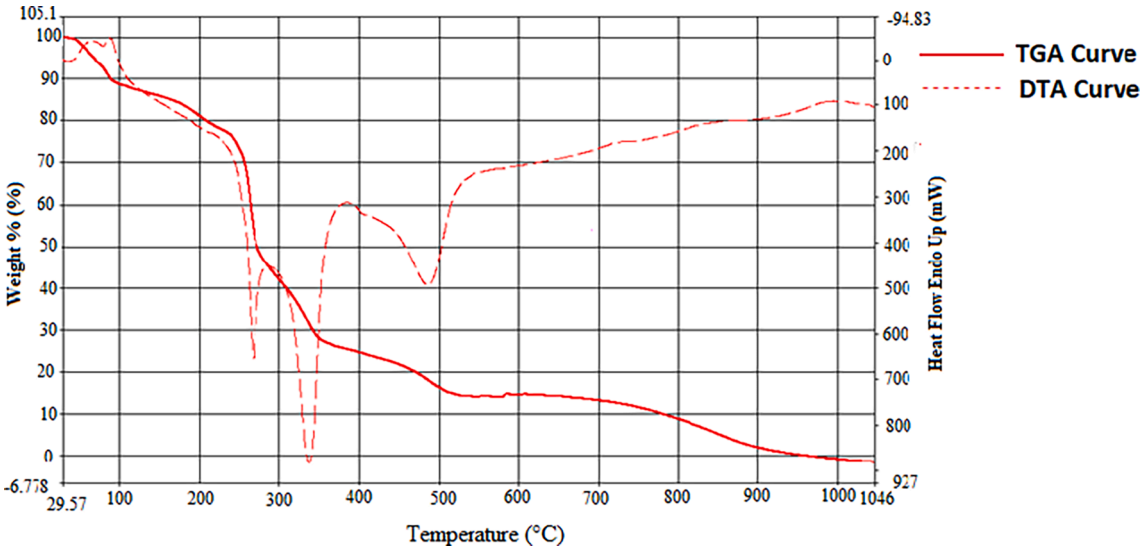

Fig. 7. TG-DTA study of the complex.

the dimensionality of the supramolecular system from 2D to 3D. Finally, the study of the present system shows that *p*H-controlled protonation can be an important factor in inducing the self-complementarity of a molecular complex which can give rise to interesting hierarchical supramolecular assembly. Role of solvent water molecules can also be an intriguing one which can still throw surprises in the form of new clusters like the hybrid water-carboxylate heptamer cluster that actively bridges metal–organic supramolecular layers in the present case. The study of this apparently simple system shows that supramolecular self-assembly is a very delicate process, even a simple protonation event can drastically influence the course of the self-assembly. Similarly solvent water molecules will keep on posing great challenges to crystal engineers who wish to predict crystal structures of given set of molecular components through formation of yet undiscovered water nano clusters. Still, the study of simple systems like the present one, will remain as worthy undertaking and may teach us a lesson or two regarding novel aspects self-assembly process.

Declaration of Competing Interest

The authors declare that they have no known competing financial interests or personal relationships that could have appeared to influence the work reported in this paper.

Acknowledgements

This work is supported by the WBDST (Project Sanction No. 203 (Sanc.)/ST/P/S&T/15G-32/2017). ADJ also thanks WBDST for financial support (Project Sanction No. 250 (Sanc.)/ST/P/S&T/16G-47/2017).

Appendix A. Supplementary data

Electronic Supplementary Information (ESI) is available online. CCDC 1947087 contains the supplementary crystallographic data for complex **1**. This data can be obtained free of charge via http://www.ccdc.cam.ac.uk/conts/retrieving.html, or from the Cambridge Crystallographic 20 Data Centre, 12 Union Road, Cambridge CB2 1EZ, UK; fax: +44 1223 336 033; or e-mail: deposit@ccdc.cam.ac.uk. Supplementary file contains additional results from XRD analysis, DFT computation, Hirshfeld analysis. Supplementary data to this article can be found online at https://doi.org/10.1016/j.rechem.2022.100421.

References

[1] X. Ning, X. Wang, Y. Zhang, X. Yu, D. Choi, N. Zheng, D.S. Kim, Y. Huang, Y. Zhang, J.A. Rogers, Assembly of advanced materials into 3D functional structures by methods inspired by origami and kirigami: A review, Adv. Mater. Interfaces 5 (2018) 1–13, https://doi.org/10.1002/admi.201800284.
[2] A.L. Dequan, Molecular Self-Assembly: Advances and Applications, CRC Press, 2012.
[3] S. Zhang, Emerging biological materials through molecular self-assembly, Biotechnol. Adv. 20 (2002) 321–339, https://doi.org/10.1016/S0734-9750(02)00026-5.
[4] J. Zhan, Y. Cai, S. He, L. Wang, Z. Yang, Tandem molecular self-assembly in liver cancer cells, Angew. Chem. 130 (2018) 1831–1834, https://doi.org/10.1002/ange.201710237.
[5] C. Yi, D. Liu, M. Yang, Building nanoscale architectures by directed synthesis and self-assembly, Curr. Nanosci. 5 (2009) 75–87, https://doi.org/10.2174/157341309787314647.
[6] L. Zang, Y. Che, J.S. Moore, One-dimensional self-assembly of planar π-conjugated molecules: Adaptable building blocks for organic nanodevices, Acc. Chem. Res. 41 (2008) 1596–1608, https://doi.org/10.1021/ar800030w.
[7] J.D. Dunitz, Thoughts on crystals as supermolecules, Cryst. Supramol. Entity (1996) 1.
[8] G.R. Desiraju, Crystal engineering: From molecule to crystal, J. Am. Chem. Soc. 135 (2013) 9952–9967, https://doi.org/10.1021/ja403264c.
[9] G.R. Desiraju, Crystal engineering: A holistic view, Angew. Chemie - Int. Ed. 46 (2007) 8342–8356, https://doi.org/10.1002/anie.200700534.
[10] G.R. Desiraju, J.J. Vittal, A. Ramanan, Crystal engineering a textbook, Crystallogr. Eng. A Textb. (2011) 1–23.
[11] A. Ali, M. Khalid, M.F. ur Rehman, S. Haq, A. Ali, M.N. Tahir, M. Ashfaq, F. Rasool, A.A.C. Braga, Efficient synthesis, SC-XRD, and theoretical studies of O-benzenesulfonylated pyrimidines: role of noncovalent interaction influence in their supramolecular network, ACS Omega. 5 (2020) 15115–15128. 10.1021/acsomega.0c00975.
[12] Y. Zhang, Y. Huang, J. Zhang, L. Zhu, K. Chen, J. Hao, Two unprecedented aromatic guanidines supramolecular chains self-assembled by hydrogen bonding interaction, J. Mol. Struct. 1097 (2015) 145–150, https://doi.org/10.1016/j.molstruc.2015.05.024.
[13] A. Das, A.D. Jana, S.K. Seth, B. Dey, S.R. Choudhury, T. Kar, S. Mukhopadhyay, N. J. Singh, I. Hwang, K.S. Kim, Intriguing π + −π interaction in crystal packing, J. Phys. Chem. B 114 (2010) 4166–4170, https://doi.org/10.1021/jp910129u.
[14] M.N. Ahmed, M. Madni, S. Anjum, S. Andleeb, S. Hameed, A.M. Khan, M. Ashfaq, M.N. Tahir, D.M. Gil, A. Frontera, Crystal engineering with pyrazolyl-thiazole derivatives: Structure-directing role of π-stacking and σ-hole interactions, CrystEngComm 23 (2021) 3276–3287, https://doi.org/10.1039/d1ce00256b.
[15] M. Madni, M.N. Ahmed, M. Hafeez, M. Ashfaq, M.N. Tahir, D.M. Gil, B. Galmés, S. Hameed, A. Frontera, Recurrent π-π stacking motifs in three new 4,5-dihydro-pyrazolyl-thiazole-coumarin hybrids: X-ray characterization, Hirshfeld surface analysis and DFT calculations, New J. Chem. 44 (2020) 14592–14603, https://doi.org/10.1039/d0nj02931a.
[16] L. Xu, X. Miao, X. Ying, W. Deng, Two-dimensional self-assembled molecular structures formed by the competition of van der Waals forces and dipole-dipole interactions, J. Phys. Chem. C 116 (2012) 1061–1069, https://doi.org/10.1021/jp210000e.
[17] A.M. Brizard, J.H. Van Esch, Self-assembly approaches for the construction of cell architecture mimics, Soft Matter. 5 (2009) 1320–1327, https://doi.org/10.1039/b812388h.

[18] Y. Lu, J. Liu, Smart nanomaterials inspired by biology: Dynamic assembly of error-free nanomaterials in response to multiple chemical and biological stimuli, Acc. Chem. Res. 40 (2007) 315–323, https://doi.org/10.1021/ar600053g.

[19] C.A. Palma, P. Samorì, M. Cecchini, Atomistic simulations of 2D bicomponent self-assembly: From molecular recognition to self-healing, J. Am. Chem. Soc. 132 (2010) 17880–17885, https://doi.org/10.1021/ja107882e.

[20] C. Fouquey, J.-M. Lehn, A.-M. Levelut, Molecular recognition directed self-assembly of supramolecular liquid crystalline polymers from complementary chiral components, Adv. Mater. 2 (1990) 254–257, https://doi.org/10.1002/adma.19900020506.

[21] S.C. McKellar, A.J. Graham, D.R. Allan, M.I.H. Mohideen, R.E. Morris, S. A. Moggach, The effect of pressure on the post-synthetic modification of a nanoporous metal-organic framework, Nanoscale 6 (2014) 4163–4173, https://doi.org/10.1039/c3nr04161a.

[22] P. Mahata, A. Sundaresan, S. Natarajan, The role of temperature on the structure and dimensionality of MOFs: An illustrative study of the formation of manganese oxy-bis(benzoate) structures, Chem. Commun. (2007) 4471–4473, https://doi.org/10.1039/b708060c.

[23] F. Yuan, J. Xie, H.M. Hu, C.M. Yuan, B. Xu, M.L. Yang, F.X. Dong, G.L. Xue, Effect of pH/metal ion on the structure of metal-organic frameworks based on novel bifunctionalized ligand 4′-carboxy-4,2′:6′,4″- terpyridine, CrystEngComm 15 (2013) 1460–1467, https://doi.org/10.1039/c2ce26171e.

[24] P.X. Yin, J. Zhang, Y.Y. Qin, J.K. Cheng, Z.J. Li, Y.G. Yao, Role of molar-ratio, temperature and solvent on the Zn/Cd 1,2,4-triazolate system with novel topological architectures, CrystEngComm 13 (2011) 3536–3544, https://doi.org/10.1039/c0ce00762e.

[25] T. Liu, D. Luo, D. Xu, H. Zeng, Z. Lin, Solvent induced structural variation in magnesium carboxylate frameworks, Inorg. Chem. Commun. 29 (2013) 110–113, https://doi.org/10.1016/j.inoche.2012.12.017.

[26] S.R. Choudhury, A.D. Jana, C.Y. Chen, A. Dutta, E. Colacio, H.M. Lee, G. Mostafa, S. Mukhopadhyay, pH-triggered changes in the supramolecular self-assembly of Cu (II) malonate complexes, CrystEngComm 10 (2008) 1358–1363, https://doi.org/10.1039/b802723d.

[27] S.R. Choudhury, H.M. Lee, T.-H. Hsiao, E. Colacio, A.D. Jana, S. Mukhopadhyay, Co-operation of π•••π, Cu(II)•••π, carbonyl•••π and hydrogen-bonding forces leading to the formation of water cluster mimics observed in the reassessed crystal structure of $[Cu(mal)(phen)(H_2O)]_2{\cdot}3H_2O$ (H_2mal=malonic acid, phen=1,10-phenanthroline), J. Mol. Struct. 967 (2010) 131–139, https://doi.org/10.1016/j.molstruc.2009.12.048.

[28] A.D. Jana, R. Saha, G. Mostafa, Acyclic water pentamer induces novel supramolecular ribbed sheet: Cooperativity and competitiveness of weak and covalent forces? J. Mol. Struct. 966 (2010) 64–68, https://doi.org/10.1016/j.molstruc.2009.12.009.

[29] C. Duan, M. Wei, D. Guo, C. He, Q. Meng, Crystal structures and properties of large protonated water clusters encapsulated by metal-organic frameworks, J. Am. Chem. Soc. 132 (2010) 3321–3330, https://doi.org/10.1021/ja907023c.

[30] R. Rosin, W. Seichter, A. Schwarzer, M. Mazik, 1,8-Naphthyridinecarbaldehydes and their methyl-substituted precursors: synthesis, molecular structures, supramolecular motifs and trapped water clusters, Eur. J. Org. Chem. 2017 (2017) 6038–6051, https://doi.org/10.1002/ejoc.201701193.

[31] G.M. Sheldrick, Crystal structure refinement with SHELXL, Acta Crystallogr. Sect. C Struct. Chem. 71 (2015) 3–8, https://doi.org/10.1107/S2053229614024218.

[32] M.A. Spackman, J.J. McKinnon, Fingerprinting intermolecular interactions in molecular crystals, CrystEngComm 4 (2002) 378–392, https://doi.org/10.1039/b203191b.

[33] P.A. Wood, J.J. McKinnon, S. Parsons, E. Pidcock, M.A. Spackman, Analysis of the compression of molecular crystal structures using Hirshfeld surfaces, CrystEngComm 10 (2008) 368–376, https://doi.org/10.1039/b715494a.

[34] M. Ashfaq, K.S. Munawar, M.N. Tahir, N. Dege, M. Yaman, S. Muhammad, S. S. Alarfaji, H. Kargar, M.U. Arshad, Synthesis, crystal structure, Hirshfeld surface analysis, and computational study of a novel organic salt obtained from benzylamine and an acidic component, ACS Omega 6 (2021) 22357–22366, https://doi.org/10.1021/acsomega.1c03078.

[35] M. Haroon, T. Akhtar, M. Yousuf, M.N. Tahir, L. Rasheed, S.S. Zahra, I. ul Haq, M. Ashfaq, Synthesis, crystal structure, Hirshfeld surface investigation and comparative DFT studies of ethyl 2-[2-(2-nitrobenzylidene)hydrazinyl]thiazole-4-carboxylate, BMC Chem. 16 (2022) 1–17, https://doi.org/10.1186/s13065-022-00805-1.

[36] M. Ashfaq, M. Khalid, M.N. Tahir, A. Ali, M.N. Arshad, A.M. Asiri, Synthesis of crystalline fluoro-functionalized imines, single crystal investigation, Hirshfeld surface analysis, and theoretical exploration, ACS Omega 7 (2022) 9867–9878, https://doi.org/10.1021/acsomega.2c00288.

[37] A. Taia, B. El Ibrahimi, F. Benhiba, M. Ashfaq, M.N. Tahir, M. Essaber, A. Aatif, T. Hökelek, J.T. Mague, N.K. Sebbar, E.M. Essassi, Syntheses, single crystal X-ray structure, Hirshfeld surface analyses, DFT computations and Monte Carlo simulations of New Eugenol derivatives bearing 1,2,3-triazole moiety, J. Mol. Struct. 1234 (2021) 130189, https://doi.org/10.1016/j.molstruc.2021.130189.

[38] J.J. McKinnon, A.S. Mitchell, M.A. Spackman, Hirshfeld surfaces: A new tool for visualising and exploring molecular crystals, Chem. Eur. J. 4 (1998) 2136–2141, https://doi.org/10.1002/(SICI)1521-3765(19981102)4:11<2136::AID-CHEM2136>3.0.CO;2-G.

[39] A.L. Rohl, M. Moret, W. Kaminsky, K. Claborn, J.J. McKinnon, B. Kahr, Hirshfeld surfaces identify inadequacies in computations of intermolecular interactions in crystals: Pentamorphic 1,8-dihydroxyanthraquinone, Cryst. Growth Des. 8 (2008) 4517–4525, https://doi.org/10.1021/cg8005212.

[40] S.K. Seth, D. Sarkar, A.D. Jana, T. Kar, On the possibility of tuning molecular edges to direct supramolecular self-assembly in coumarin derivatives through cooperative weak forces: Crystallographic and hirshfeld surface analyses, Cryst. Growth Des. 11 (2011) 4837–4849, https://doi.org/10.1021/cg2006343.

[41] M. Ashfaq, M.N. Tahir, S. Muhammad, K.S. Munawar, S. Ali, G. Ahmed, A.G. Al-Sehemi, S.S. Alarfaji, M.E. Ibraheem Khan, Shedding light on the synthesis, crystal structure, characterization, and computational study of optoelectronic properties and bioactivity of imine derivatives, ACS Omega 7 (2022) 5217–5230, https://doi.org/10.1021/acsomega.1c06325.

[42] D., W. S. K., G. D. J., M. J. J., Jayatilaka, M.A. Spackman, Crystal Explorer 2.1 University of Western Australia: Perth, Australia, 2007, (n.d.).

[43] H. Mehmood, M. Khalid, M. Haroon, T. Akhtar, M. Ashfaq, M.N. Tahir, M.U. Khan, M. Imran, A.A.C. Braga, S. Woodward, Synthesis, characterization and DFT calculated properties of electron-rich hydrazinylthiazoles: Experimental and computational synergy, J. Mol. Struct. 1245 (2021) 131043, https://doi.org/10.1016/j.molstruc.2021.131043.

[44] M. Ashfaq, A. Ali, A. Kuznetsov, M.N. Tahir, M. Khalid, DFT and single-crystal investigation of the pyrimethamine-based novel co-crystal salt: 2,4-diamino-5-(4-chlorophenyl)-6-ethylpyrimidin-1-ium-4-methylbenzoate hydrate (1:1:1) (DEMH), J. Mol. Struct. 1228 (2021) 129445, https://doi.org/10.1016/j.molstruc.2020.129445.

[45] A. Ali, M. Khalid, M.N. Tahir, M. Imran, M. Ashfaq, R. Hussain, M.A. Assiri, I. Khan, Synthesis of diaminopyrimidine sulfonate derivatives and exploration of their structural and quantum chemical insights via SC-XRD and the DFT approach, ACS Omega 6 (2021) 7047–7057, https://doi.org/10.1021/acsomega.0c06323.

[46] A. Ali, A. Kuznetsov, M. Ashfaq, M.N. Tahir, M. Khalid, M. Imran, A. Irfan, Synthesis, single-crystal exploration, and theoretical insights of arylsulfonylated 2-amino-6-methylpyrimidin derivatives, J. Mol. Struct. 1243 (2021) 130789, https://doi.org/10.1016/j.molstruc.2021.130789.

[47] A. Ali, M. Khalid, Z.U. Din, H.M. Asif, M. Imran, M.N. Tahir, M. Ashfaq, E. Rodrigues-Filho, Exploration of structural, electronic and third order nonlinear optical properties of crystalline chalcone systems: Monoarylidene and unsymmetrical diarylidene cycloalkanones, J. Mol. Struct. 1241 (2021) 130685, https://doi.org/10.1016/j.molstruc.2021.130685.

[48] J.A.P. M. J. Frisch, G. W. Trucks, H. B. Schlegel, G. E. Scuseria, M. A. Robb, J. R. Cheeseman, J. A. Montgomery, T. Vreven, K. N. Kudin, J. C. Burant, J. M. Millam, S. S. Iyengar, J. Tomasi, V. Barone, B. Mennucci, M. Cossi, G. Scalmani, N. Rega, G. A. Petersso, Gaussian 03 Package, (2003).

[49] B. Dey, S.R. Choudhury, E. Suresh, A.D. Jana, S. Mukhopadhyay, Use of π–π forces to steer the assembly of a NTA complex of Cu(II) into hydrogen bonded supramolecular layers (H_3NTA=nitrilotriacetic acid), J. Mol. Struct. 921 (2009) 268–273, https://doi.org/10.1016/j.molstruc.2009.01.004.

[50] Y. Jiang, H. Kou, R.-J. Wang, A.-L. Cui, A sandwich strand supramolecular complex: aquachloro(nitrilotriacetato-κ 2 N, O)copper(II) 18-crown-6-ether trihydrate, Acta Crystallogr. Sect. E Struct. Reports Online 62 (2006) m804–m806, https://doi.org/10.1107/S1600536806008427.

[51] B. Li, B. Li, J. Lang, Y. Zhang, A novel two-dimensional network self-assembled by the narrowest ladder cations $[Cu(CH_3COO)(bpe)(H_2O)]nn+$containing the $Cu_2(\mu\text{-}O)_2$cores and the dimeric anions $[Cu_2(nta)_2(bpe)]_2$-through hydrogen-bonding interaction, Inorg. Chem. Commun. 6 (2003) 725–727, https://doi.org/10.1016/S1387-7003(03)00093-5.

[52] B. Li, B. Li, X. Zhu, Y. Zhang, Two unusual copper complexes with nitrilotriacetate and 4,5-diazafluoren-9-one or trans-1,2-bis(4-pyridyl)ethylene mixed-ligands, Inorg. Chem. Commun. 6 (2003) 1304–1306, https://doi.org/10.1016/j.inoche.2003.08.002.

[53] J.C. and Z.X. Baolong Li, Yan Xu, Yi Dong, Synthesis and crystal structure of $[Cu(azpy)(H_2O)_4]$ $[Cu_2(nta)_2(azpy)]{\cdot}6H_2O$: A two-dimensional network solid, Chem. Informationsd. 17 (1986) 357–361. 10.1023/A:1015795722065.

[54] Z. Li Baolong, Xu, Yan, Lin, Qi, Wang, Hua-Qin, Xu, Synthesis Structure and Characterization of Two-dimensional Network Copper Complex [$Cu_3(nta)_2(azpy)(H_2O)_2$], Chinese J. Chem. 3 (2001) 187–190.

[55] S. Jana, A. D.; Maiti, The Importance of Intermolecular Interaction in Solid-state X-ray Crystal Structures., in: S.K. Seth (Ed.), 1st ed., New Academic Publisher, 2016: pp. 5–44.

[56] B. Dutta, S.R. Ghosh, A. Ray, S. Jana, C. Sinha, S. Das, A.D. Jana, M.H. Mir, Stabilization of cyclic water tetramers and dimers in the crystal host of 2D coordination networks: electrical conductivity and dielectric studies, New J. Chem. 44 (2020) 15857–15870, https://doi.org/10.1039/d0nj03750h.